

Aeroacoustic source term filtering based on Helmholtz decomposition

Stefan J. Schoder* and Manfred Kaltenbacher†

Vienna University of Technology, Vienna, Vienna, 1060, Austria

Hybrid aeroacoustic methods seek for computational efficiency and robust noise prediction. Using already existing aeroacoustic wave equations, we propose a general hybrid aeroacoustic method, based on compressible source data. The main differences to current state of the art aeroacoustic analogies are that an additional decomposition is used to compute the aeroacoustic source terms and their application is extended to the source formulation, based on compressible flow data. By applying the Helmholtz-Hodge decomposition on arbitrary domains, we extract the incompressible projection (non-radiating base flow) of a compressible flow simulation. This method maintains the favorable properties of the hybrid aeroacoustic method while incorporating compressible effects on the base flow. The capabilities are illustrated for the aeroacoustic benchmark case, "cavity with a lip", involving acoustic feedback. The investigation is based on the equation of vortex sound, to incorporate convective effects during wave propagation.

Nomenclature

\mathbf{A}	Vector potential	ϕ	Scalar potential
H	Specific enthalpy	ρ	Density
\mathbf{I}	Identity tensor	$\boldsymbol{\tau}$	Stress tensor
\mathbf{L}	Lamb vector	$\boldsymbol{\omega}$	Vorticity
R_s	Specific gas constant	\star	Generic field variable
SPL	Sound pressure level	<i>Subscript</i>	
T	Temperature	d	Depth mode
\mathbf{T}	Lighthill tensor	s	Shear layer mode
U_∞	Free stream velocity	<i>Superscript</i>	
c	Isentropic speed of sound	a	Compressible part
f	Frequency	c	Compressible part
p	Pressure	h	Harmonic part
p_0	Reference pressure	ic	Incompressible part
\mathbf{u}	Fluid velocity	*	Joint function
Γ	Boundary	'	Radiating fluctuation
Ω	Domain	~	Non-radiating base flow
δ	Boundary layer thickness		

I. Introduction

In modern transport systems, passengers' comfort is greatly influenced by flow induced noise. The cavity with a lip represents a generic model of a vehicle door gap, involving an acoustic feedback mechanism on the underlying flow field. Even though, great advances have been made in direct computation of aerodynamic sound, a Direct Numerical Simulation with commercial solvers, fully resolving flow and acoustic quantities

*Doctoral candidate, Institute of Mechanics and Mechatronics, Vienna.

†Full Professor, Institute of Mechanics and Mechatronics, Vienna, and AIAA Member Senior.

is infeasible for most practical applications. Within our contribution, a hybrid computational aeroacoustic (CAA) approach combines the strength of a compressible flow simulation with the application of an aeroacoustic analogy based on compressible flow data.

The first proposed acoustic analogy by Lighthill^{1,2} transforms the compressible Navier-Stokes equation into an exact inhomogeneous wave equation. A preferable source term modeling is based on the incompressible flow simulation,³ since wave propagation is omitted in the incompressible flow simulation. Several modifications of Lighthill's source term were extensively used for low Mach number applications. These methods implicitly describe a one-way coupling from flow structures to acoustic waves. Since then, exact and computationally efficient source term formulations, conforming with the flow simulation are investigated. In the context of modeling aeroacoustic source terms, a first breakthrough was reached when deriving a proper non-linear source term of the linearized Euler equations.⁴ Ewert proposed a filtering technique to extract pure source terms of a compressible flow simulation to force the acoustic perturbation equations (APE) formulation.⁵ Assuming a compressible flow simulation, the flow field already incorporates wave propagation, corrupting the source term computation based on the compressible flow data.⁶ Goldstein⁷ proposed an additive splitting in a radiating and non-radiating base flow. He stated that "*A possible non-radiating base flow is an incompressible flow*", which can be utilized to construct pure acoustic source terms.

Some practical applications (e.g. cavity with a lip, resonator-like structures) seek for compressible simulations, since acoustic feedback mechanisms excite flow structures.⁸ Currently available commercial tools suggest sponge layers as absorbing boundary conditions and apply, in most cases, first and second order accurate numerical schemes. Therefore, the overall compressible flow field (including vortices and waves) is modeled inappropriately during the flow simulation and corrupts the acoustic source term calculation. The main challenge is to filter the flow field, such that the non-radiating component is extracted. As Goldstein⁷ proposed, a representation of a non-radiating source field is the incompressible flow. This incompressibility condition gives rise to a Helmholtz decomposition of the compressible flow field. First results of the methodology and computations, also considered here, have been published.⁹

II. Formulation

A general aeroacoustic analogy assumes a causal forward coupling of the forcing (obtained by an independent flow simulation) on fluctuating quantities, e.g. the fluctuating pressure p' , which approaches the acoustic pressure p^a at large distances from the turbulent region. Thereby, a general acoustic analogy composes a hyperbolic left hand side defined by a wave operator and a generic right hand side **RHS**(\star)

$$\square p' = \mathbf{RHS}(p, \mathbf{u}, \rho, \dots). \quad (1)$$

To this end, Lighthill's inhomogeneous wave equation perfectly fits to this class, which reads as^{1,2}

$$\frac{\partial^2 \rho'}{\partial t^2} - c_0^2 \nabla \cdot \nabla \rho' = \nabla \cdot \nabla \cdot [\mathbf{T}]. \quad (2)$$

In (2) ρ' denotes the density fluctuation, c_0 the constant speed of sound and the entries of the Lighthill tensor $[\mathbf{T}]$ compute by

$$[\mathbf{T}] = \rho \mathbf{u} \mathbf{u} + \left((p - p_0) - c_0^2 (\rho - \rho_0) \right) [\mathbf{I}] - [\boldsymbol{\tau}] \quad (3)$$

with the fluid velocity \mathbf{u} , the pressure and density fluctuations $p' = p - p_0$, $\rho' = \rho - \rho_0$ and the viscous stresses τ_{ij} . It is obvious that the right hand side **RHS**(\star) of Lighthill's inhomogeneous wave equation contains not only source terms, but also interaction terms between the sound and flow field, which includes effects as convection and refraction of the sound by the flow. Therefore, the whole set of compressible flow dynamics equations have to be solved in order to calculate the right hand side of (2). However, this means that we have to resolve both the flow structures and acoustic waves, which is an enormous challenge for any numerical scheme and the computational noise itself may strongly disturb the physical radiating wave components.¹⁰ Therefore, in the theories of Phillips and Lilley interaction effects have been, at least to some extend, moved to the wave operator \square .^{11,12} These equations predict certain aspects of the sound field surrounding a jet quite accurately, which are not accounted for Lighthill's equation due to the restricted numerical resolution of the source term in (2).¹³ For low Mach number flows, an incompressible flow simulation to obtain the source field can be applied, and we can construct the source terms based on this non-radiating base flow. E.g., Lighthill's tensor reduces to

$$[\mathbf{T}] = \rho_0 \mathbf{u}^{\text{ic}} \mathbf{u}^{\text{ic}} \quad (4)$$

with the incompressible flow velocity \mathbf{u}^{ic} . This promising and most favorable coupling of aeroacoustic analogy is widely used and shows accurate results as long as the flow simulation resolves the physics (since the assumptions of the incompressible flow simulation and the acoustic analogy are both satisfied - no feedback). The incompressible flow simulation constrains the capabilities of a hybrid methodology for aeroacoustic analogies to very low Mach numbers and cases, where the influence of the acoustic on the flow field can be neglected. In 2003, Goldstein⁷ proposed a method to split flow variables (p, \mathbf{u}, \dots) into a base flow (non-radiating) and a remaining component (acoustic, radiating fluctuations)

$$\star = \tilde{\star} + \star' . \quad (5)$$

Applying the decomposition to the right hand side of the wave equation (the left hand side of the equation is already treated in this manner during the derivation of the acoustic analogy) leads to

$$\square p' = \mathbf{RHS}(\tilde{p}, \tilde{\mathbf{u}}, \tilde{\rho}, p', \mathbf{u}', \rho', \dots) . \quad (6)$$

Now interaction terms can be moved to the differential operator to take, e.g., convection and refraction effects or even nonlinear interactions into account. Exactly this approach has been applied in the theories of Phillips and Lilley, and furthermore in the derivation of perturbation equations.^{5,14,15} E.g., the APE⁵ based on incompressible flow data result in the following system of equations for the acoustic pressure p^{a} and acoustic particle velocity \mathbf{u}^{a}

$$\begin{aligned} \frac{\partial p^{\text{a}}}{\partial t} + \bar{\mathbf{u}} \cdot \nabla p^{\text{a}} + \bar{\rho} c_0^2 \nabla \cdot \mathbf{u}^{\text{a}} &= -\frac{\partial p^{\text{ic}}}{\partial t} - \bar{\mathbf{u}} \cdot \nabla p^{\text{ic}} \\ \bar{\rho} \frac{\partial \mathbf{u}^{\text{a}}}{\partial t} + \bar{\rho} \nabla (\bar{\mathbf{u}} \cdot \mathbf{u}^{\text{a}}) + \nabla p^{\text{a}} &= 0 \end{aligned} \quad (7)$$

or equivalently reformulated by the perturbed convective wave equation (PCWE)¹⁶

$$\square \psi^{\text{a}} = \frac{1}{c^2} \frac{D^2 \psi^{\text{a}}}{Dt^2} - \Delta \psi^{\text{a}} = -\frac{1}{\bar{\rho} c_0^2} \frac{D p^{\text{ic}}}{Dt} ; \quad \frac{D}{Dt} = \frac{\partial}{\partial t} + \bar{\mathbf{u}} \cdot \nabla \quad (8)$$

with the acoustic scalar potential ψ^{a} , mean flow velocity $\bar{\mathbf{u}}$ and mean density $\bar{\rho}$. The application to a cylinder in cross flow at a Mach number of 0.3 showed that simulations based on compressible flow data overestimated the acoustic pressure by a factor of 3 as compared by using the incompressible pressure p^{ic} in the source term.⁵

Referring to Goldstein's concept, we aim to relax the Mach number constraint imposed by the incompressible flow simulation. Naturally, this leads to a compressible flow simulation. Acoustics and other radiating components are already incorporated in the flow quantities, composing the right hand side of the wave equation. However, from a physical and mathematical aspect, these quantities are modeled by the left hand side operator and its properties. In,⁷ Goldstein proposed different approaches of deriving a base flow about which the linearized equations for the radiating quantities are obtained. Since in most flows, even in high speed flows the radiated sound is typically orders of magnitude smaller than the non-radiating components, one should separate out radiating components of the motion to achieve a base flow, which is described entirely by non-radiating components. Therefore, we propose the three steps to relax the Mach number constraint imposed by the incompressible flow simulation. First, we perform a compressible flow simulation, which incorporates two-way coupling of the flow and acoustics and extends aeroacoustic analogies to physical phenomena, where feedback matters. Second, we assume that the main interaction terms between the flow and the acoustic field are modeled by the wave operator, e.g. convection and refraction effects as in the case of (7), (8). Third, we filter the aeroacoustic sources, such that we obtain a pure non-radiating field that computes the sources and solve with an appropriate wave operator for the radiating field

$$\square p' = \mathbf{RHS}(\tilde{p}, \tilde{\mathbf{v}}, \tilde{\rho}, \dots) . \quad (9)$$

Thereby, the non-radiating base flow is obtained by applying a Helmholtz-Hodge decomposition (see Sec. B). Our approach is of strong practical relevance, since state of art commercial flow solvers are just second order accurate in space and time and do not provide a computational boundary treatment, which is capable to absorb both vortices and waves without reflections. Due to these shortcomings numerical dispersion

results in un-physical wave damping and the limited computational domain may lead to un-physical domain resonances. However, we also want to note that a direct numerical simulation solving the compressible flow dynamics equations and resolving both vortices and waves does not need any approximations in the modeling and includes all physical interaction and source mechanism effects. The obtained physical quantities are total pressure, velocity, density, etc. and are composed of both radiating and non-radiation components. So, also in this case a decomposition into radiating and non-radiation components may be of great interest, which can be performed by the Helmholtz-Hodge decomposition as described in Sec. B.

A. Aeroacoustic analogy

The equation of vortex sound¹⁷ derived from Crocco's form of the momentum equation is based on the total enthalpy

$$H = \int \frac{dp}{\rho} + \frac{u^2}{2} \quad (10)$$

as primary variable, with $u^2 = \mathbf{u} \cdot \mathbf{u}$. The acoustic analogy for homentropic flow reads as

$$\frac{1}{c^2} \frac{D^2}{Dt^2} H - \nabla \cdot \nabla H = \nabla \cdot (\boldsymbol{\omega} \times \mathbf{u}) = \nabla \cdot \mathbf{L}(\mathbf{u}), \quad (11)$$

where for a constant isentropic speed of sound c and density ρ_0 the equation demonstrates the relevancy of the vorticity as aeroacoustic source term. The wave operator is of convective type, where the total derivative (material derivative) is defined as $\frac{D\star}{Dt} = \frac{\partial\star}{\partial t} + (\mathbf{u} \cdot \nabla)\star$. The fluid velocity \mathbf{u} is generally considered as the velocity of a compressible fluid motion, where $\boldsymbol{\omega} = \nabla \times \mathbf{u}$ describes the vorticity of the fluid. The application of this aeroacoustic analogy is valid for large Reynolds number flows. The aeroacoustic source term is known as the divergence of the Lamb vector \mathbf{L}

$$\mathbf{L}(\mathbf{u}) = (\boldsymbol{\omega} \times \mathbf{u}). \quad (12)$$

In the present method we aim to filter out parasitic effects (acoustics and other numerical radiating components) of the source flow field, which occur due to the compressible flow simulation and have no physical origin. The filtered quantities describe the physical field without boundary artifacts and propagating waves due to the compressible fluid in the flow simulation. Thus, we reformulate the Lamb vector in terms of the non-radiating base flow $\tilde{\mathbf{u}}$, as follows

$$\mathbf{L}(\tilde{\mathbf{u}}) = (\boldsymbol{\omega} \times \tilde{\mathbf{u}}). \quad (13)$$

Applying the correction of the aeroacoustic source term to the equation of vortex sound (11), we obtain the wave equation with the filtered source term. Finally, we arrive at the inhomogeneous wave equation in terms of the total enthalpy

$$\frac{1}{c^2} \frac{D^2}{Dt^2} H - \nabla \cdot \nabla H = \nabla \cdot \mathbf{L}(\tilde{\mathbf{u}}). \quad (14)$$

B. Helmholtz-Hodge decomposition

As already outlined, some practical applications seek for a compressible flow simulation, to consider acoustic feedback mechanisms on the flow structures. However, the state of the art boundary conditions and the applied numerical schemes used in commercial flow simulation tools cause additional artificial effects, like domain resonances of the compressible phenomena. Naturally, the incompressibility condition (regarding the concept of a non-radiating base flow of Goldstein) leads to the Helmholtz-Hodge decomposition of the flow field. Similar to the decomposition of perturbation equations, we propose an additive splitting on the bounded problem domain Ω of the velocity field $\mathbf{u} \in L^2(\Omega)$ in L^2 -orthogonal velocity components

$$\mathbf{u} = \mathbf{u}^{\text{ic}} + \mathbf{u}^{\text{c}} + \mathbf{u}^{\text{h}} = \nabla \times \mathbf{A}^{\text{ic}} + \nabla \phi^{\text{c}} + \mathbf{u}^{\text{h}}, \quad (15)$$

where \mathbf{u}^{ic} represents the solenoidal (incompressible, non-radiating base flow) part, \mathbf{u}^{c} the irrotational (compressible, radiating) part and \mathbf{u}^{h} the harmonic (divergence-free and curl-free) part of the flow velocity. We investigate two possible computations of the base flow \mathbf{u}^{ic} . The scalar potential ϕ^{c} is associated with the compressible part and the property $\nabla \times \mathbf{u}^{\text{c}} = 0$, whereas the vector potential \mathbf{A}^{ic} describes the incompressible part of the velocity field, satisfying $\nabla \cdot \mathbf{u}^{\text{ic}} = 0$. These properties lead to a scalar Poisson problem for the scalar potential ϕ^{c} with the rate of expansion $\nabla \cdot \mathbf{u}$ as forcing and to a curl-curl problem with $\nabla \times \mathbf{u}$ as right hand side when seeking for \mathbf{A}^{ic} , respectively.

Based on the decomposition (15) we formulate the actual computation of the additive velocity components for a bounded domain, where the compressible flow field \mathbf{u} and its derivatives do not decay towards or vanish at the boundaries of the decomposition domain. Thus, we have to include the harmonic part \mathbf{u}^h of the decomposition. The harmonic part is the homogeneous solution of the partial differential equation and physically speaking the potential flow solution of the configuration. The decomposition domain is depicted in Fig. 3, with the flow boundaries $\Gamma_{1,\dots,4}$.

C. Poisson's equation for the scalar potential

The scalar potential $\phi^{*,c} \in \mathcal{V} = \{\varphi \in H^1(\Omega) | \nabla \varphi \cdot \mathbf{n} = \mathbf{u} \cdot \mathbf{n} \text{ on } \Gamma_{2,4}, \varphi = 0 \text{ on } \Gamma_{1,3}\}$ is associated with the compressible part and the property $\nabla \times \mathbf{u}^{*,c} = 0$. The star denotes the joint function of both parts, the compressible and the harmonic component. Thus, we construct the decomposition as

$$\mathbf{u} = \nabla \times \mathbf{A}^{ic} + \nabla \phi^{*,c} \quad (16)$$

$$\nabla \phi^{*,c} = \mathbf{u}^{*,c} = \mathbf{u}^c + \mathbf{u}^h = \nabla \phi^c + \nabla \phi^h. \quad (17)$$

By taking the divergence of equation (16) we obtain a scalar valued Poisson equation with the rate of expansion $\nabla \cdot \mathbf{u}$ as forcing

$$\nabla \cdot \nabla \phi^{*,c} = \nabla \cdot \mathbf{u}. \quad (18)$$

The decomposition comes along with suitable boundary conditions, due to the space \mathcal{V} and orthogonality condition

$$\int_{\Gamma} \phi^{*,c} \mathbf{u}^{ic} \cdot \mathbf{n} ds = 0, \quad (19)$$

ensuring the orthogonality of the components. Having this in mind, we adjust the boundaries to ensure a unique decomposition. We gain the non-radiating component of the compressible flow \mathbf{u} by subtracting the radiating components

$$\tilde{\mathbf{u}} := \mathbf{u} - \nabla \phi^{*,c}. \quad (20)$$

D. Curl-Curl equation for the vector potential

Analogously to the scalar potential, the vector potential $\mathbf{A}^{*,ic} \in \mathcal{W} = \{\varphi \in H(curl, \Omega) | \mathbf{n} \times \nabla \times \varphi = \mathbf{n} \times \mathbf{u} \text{ on } \Gamma_{1,2,3,4}\}$ is associated with the incompressible part and the property $\nabla \cdot \mathbf{u}^{*,ic} = 0$. The star again denotes the joint function of both parts, the incompressible and the harmonic one.

$$\mathbf{u} = \nabla \times \mathbf{A}^{*,ic} + \nabla \phi^c \quad (21)$$

$$\nabla \times \mathbf{A}^{*,ic} = \mathbf{u}^{*,ic} = \mathbf{u}^{ic} + \mathbf{u}^h = \nabla \times \mathbf{A}^c + \nabla \times \mathbf{A}^h \quad (22)$$

By taking the curl of equation (21) we obtain a vector valued curl-curl equation (similar to magnetostatics) with the vorticity $\boldsymbol{\omega} = \nabla \times \mathbf{u}$ as forcing

$$\nabla \times \nabla \times \mathbf{A}^{*,ic} = \nabla \times \mathbf{u} = \boldsymbol{\omega}. \quad (23)$$

The function space \mathcal{W} for the vector potential requires a finite element discretization with edge elements (Nédélec elements). Due to the space \mathcal{W} and the orthogonality condition, the decomposition comes along with a suitable boundary condition

$$\int_{\Gamma} \mathbf{A}^{*,ic} \cdot (\mathbf{u}^c \times \mathbf{n}) ds = 0, \quad (24)$$

ensuring the orthogonality of the components and a unique decomposition. Finally, we obtain the non-radiating component, which contains all divergence-free components, as

$$\tilde{\mathbf{u}} := \mathbf{u}^{*,ic} = \nabla \times \mathbf{A}^{*,ic}. \quad (25)$$

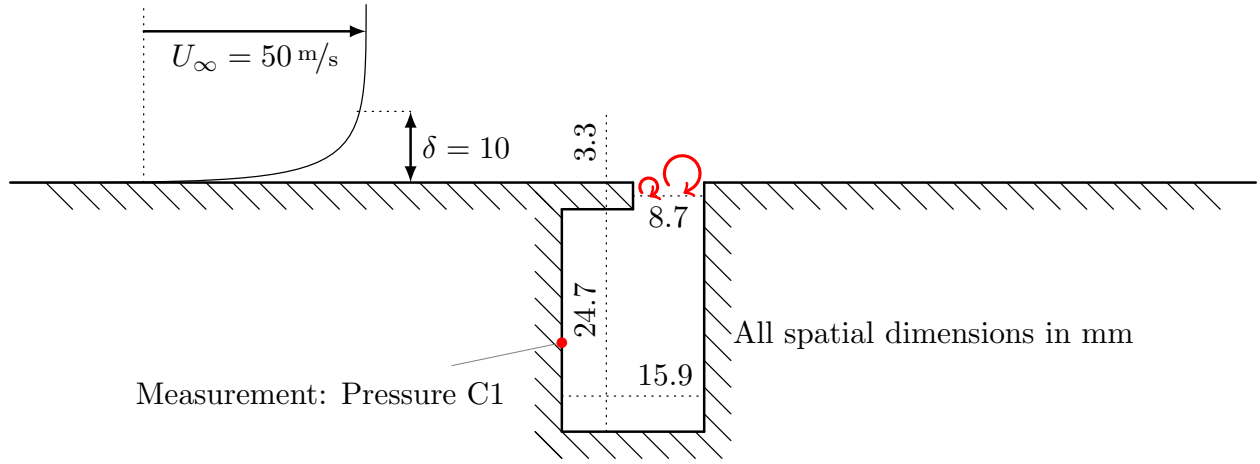


Figure 1. The geometry and the flow configuration of the benchmark problem, cavity with a lip.

III. Application example

We demonstrate the proposed method for the aeroacoustic benchmark case,¹⁸ "cavity with a lip". The geometrical properties are given in Fig. 1, with all spatial dimensions in mm. The deep cavity has a reduced cross-section at the orifice (Helmholtz resonator like geometry) and the cavity separates two flat plate configurations. The Helmholtz resonance of the cavity is about 4400 Hz, such that no pressure fluctuations in the boundary layer excite the resonator. The flow, with a free-stream velocity of $U_\infty = 50 \text{ m/s}$, develops over the plate up to a boundary layer thickness of $\delta = 10 \text{ mm}$. For this configuration we expect a depth mode in the cavity at about $f_d = 1400 \text{ Hz}$ and a first shear layer mode at $f_{s1} = 1700 \text{ Hz}$. The expected resonance frequencies are well captured by measurements (see Fig. 2).

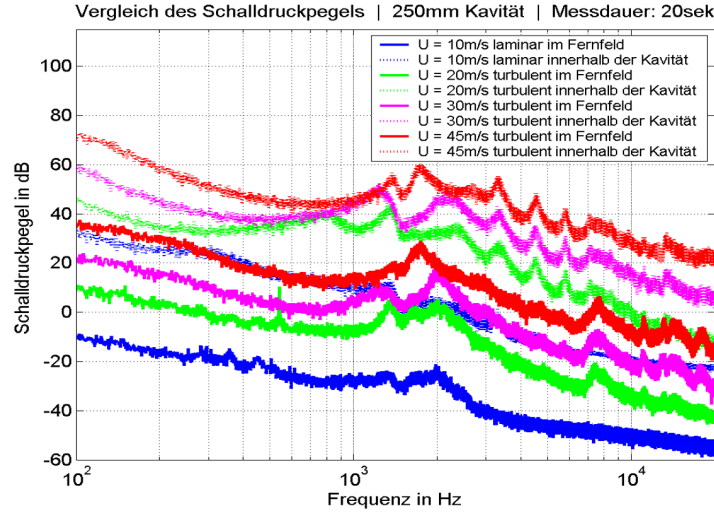


Figure 2. Experimental investigation of the cavity with a lip for various boundary layer free stream velocities. The study was conducted at Friedrich Alexander University Erlangen during a diploma thesis.¹⁹

IV. Simulation results

The aeroacoustic benchmark case, cavity with a lip, is investigated and we determine the acoustic field, resulting from a hybrid aeroacoustic simulation based on compressible flow data. The workflow is split in three main steps. At first, a compressible flow simulation on a reduced domain Ω_F is carried out, such

that the flow phenomena is captured. The second computation filters the compressible flow data on the flow domain Ω_F and extracts the non-radiating base flow in order to construct the vortical source term \mathbf{L} . Finally, the acoustic propagation is computed on the joint spatial domain $\Omega_A = \Omega_P \cup \Omega_F$ both in frequency and time domain (see Fig. 3). The perfectly matching layer serves as an accurate free field radiation condition.

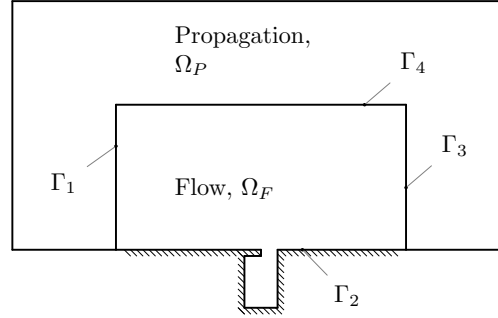


Figure 3. The flow domain Ω_F is a subdomain of the acoustic domain Ω_A , which includes the flow domain as its source domain and the propagation domain Ω_P .

A. Fluid dynamics

We performed compressible as well as incompressible flow simulations of the cavity with a lip on the 2D domain Ω_F . Since the expected modes (f_d, f_{s1}) involve strong feedback mechanisms from the compressible part of the solution on the vortical structures, a compressible simulation is crucial. A compressible flow simulation predicts the modes in the range of 1000 Hz to 2000 Hz accurately (see Fig. 4). Measurements confirm the simulation results. An incompressible simulation misinterprets the physics and predicts a shear layer mode of second type.⁸ The unsteady, compressible, and laminar flow simulation is performed with a prescribed velocity profile $\mathbf{u} = \mathbf{u}_{in}$ at the inlet Γ_1 , a no slip and no penetration condition $\mathbf{u} = \mathbf{0}$ for the wall Γ_2 , an enforced reference pressure $p = p_{ref}$ at the outlet Γ_3 , and a symmetry condition $\mathbf{u} \cdot \mathbf{n} = 0$ at the top Γ_4 (see Fig. 3).

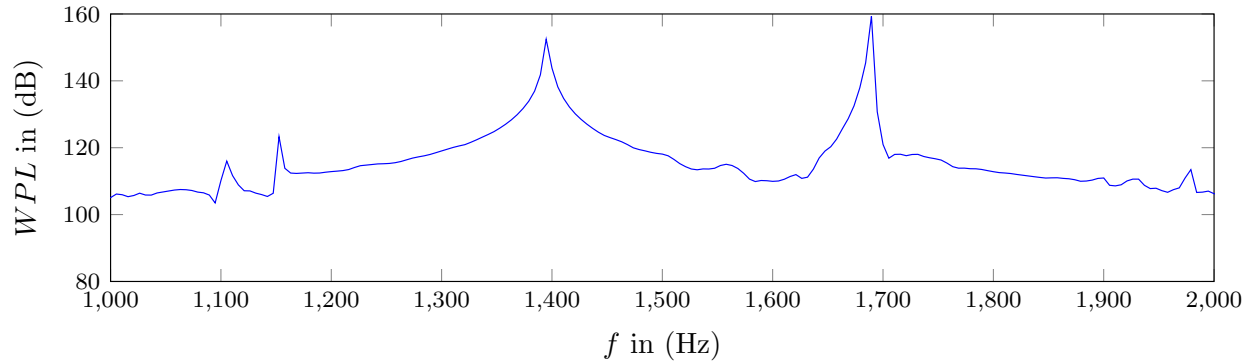


Figure 4. The wall pressure level (WPL) of the compressible flow simulation at the observation point C1 in the cavity. Two physical modes are located at 1400Hz and 1680Hz (1st shear layer mode) and the artificial computational domain resonances are located around 1100Hz. The reference pressure is 20 μ Pa.

Figure 5 shows the rate of expansion $\nabla \cdot \mathbf{u}$ of the compressible flow simulation at a representative time step. The artificial computational domain resonances are dominant in the whole domain and excite compressible effects at a frequency of about 1150 Hz (see Fig. 4). This shows how important it is to model boundaries with respect to the physical phenomena. A direct numerical simulation using a commercial flow solver, resolving flow and acoustic, suffers the following main drawbacks. First, transmission boundaries for vortical and wave structures are limited and often inaccurate. In computational fluid dynamics the boundaries are optimized to propagate vortical structures without reflection. But in contrast to that, the radiation condition of waves are not modeled precisely and, as depicted in Fig. 5, artificial computational domain resonances superpose the dominant flow field. The state of the art modeling approach in flow simulation utilizes sponge

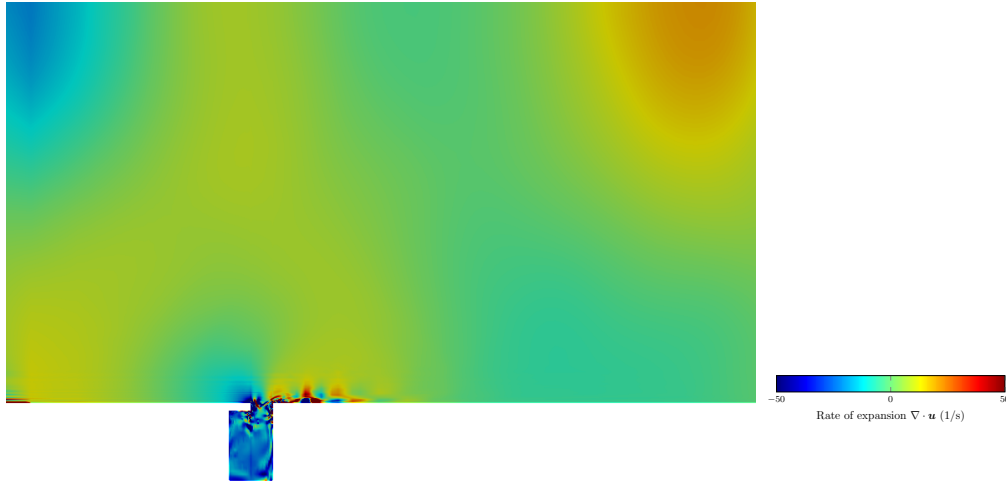


Figure 5. The rate of expansion $\nabla \cdot \mathbf{u}$ of the compressible flow simulation at a representative time step. The figure demonstrates the presence of standing waves due to the boundary conditions of the compressible flow simulation.

layer techniques, to damp acoustic waves towards the boundaries, so that they have no influence on the simulation with respect to the wave modeling. Second, low order accuracy of currently available commercial flow simulation tools and the numerical damping dissipates the waves before they are propagated into the far field. Third, a relatively high computational cost to resolve both flow and acoustics exists.

The Helmholtz-Hodge decomposition of the flow field aims to extract this artificial computational domain resonances due to the boundary condition at $\Gamma_1, \Gamma_3, \Gamma_4$. Furthermore, the decomposition extracts physical radiating compressibility such that the non-radiating base flow is obtained.

B. Helmholtz-Hodge decomposition

Both, the scalar and the vector potential formulation have been implemented applying the finite element method. The simply connected domain Ω_F , with its reentrant corners at the orifice of the cavity, causes singularities in the compressible velocity component $\mathbf{u}^{*,c} = \nabla \phi^{*,c}$ (see Fig. 6). This holds for domains, where corners with a corner angle $\theta > \pi$ exist. The singularities can be treated by a graded mesh. Overall, the L^2 -orthogonality

$$\langle \nabla \phi^{*,c}, \mathbf{u} - \nabla \phi^{*,c} \rangle := \int_{\Omega_F} \phi^{*,c} \cdot (\mathbf{u} - \nabla \phi^{*,c}) dx = 6 \cdot 10^{-4}\% \quad (26)$$

of the extracted field $\nabla \phi^{*,c}$ to the complementary field $\mathbf{u} - \nabla \phi^{*,c}$ holds.

In contrast to the scalar potential formulation, the configuration of the vector potential (Fig. 7) does not face singularities at the corners. The L^2 orthogonality of the extracted field $\nabla \times \mathbf{A}^{*,ic}$ to the complementary field $\mathbf{u} - \nabla \times \mathbf{A}^{*,ic}$ holds, $\langle \nabla \times \mathbf{A}^{*,ic}, \mathbf{u} - \nabla \times \mathbf{A}^{*,ic} \rangle = 0.02\%$.

As the boundaries for both calculation procedures are adjusted to the orthogonality condition at the boundaries (19) and (24), our approach is able to extract a unique pair of L^2 orthogonal vector fields $\langle \nabla \times \mathbf{A}^{*,ic}, \nabla \phi^{*,c} \rangle = 0.03\%$. Finally, the decomposed field allows us to calculate the corrected aeroacoustic source term. In the case of the reentrant corners, we prefer the usage of the vector potential, since no singularities are present and the overall extracted field contains all divergence-free components.

C. Acoustic propagation

This method tackles the compressible phenomena inside the domain Ω_F by filtering the domain artifacts of the compressible flow field such that the computed sources are not corrupted. The result of the vector potential formulation is used to construct the corrected Lamb vector $\mathbf{L}(\tilde{\mathbf{u}})$ (Fig. 8.a). The equation of vortex sound is solved for the total enthalpy H in terms of the finite element method by the in-house solver CFS++.²⁰ We investigate the effectiveness of the filtering technique of the overall acoustic propagation in

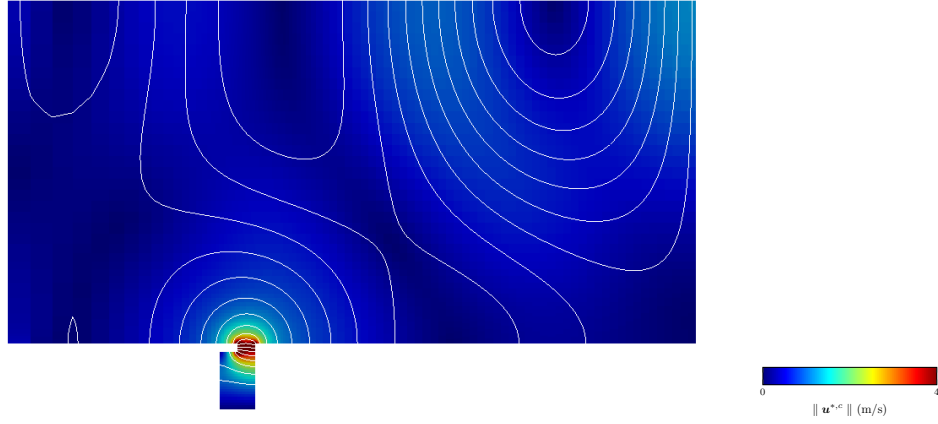


Figure 6. The magnitude of the compressible part of the velocity reveals the singularities in the orifice of the cavity. As illustrated the artificial pattern in the domain is captured well.

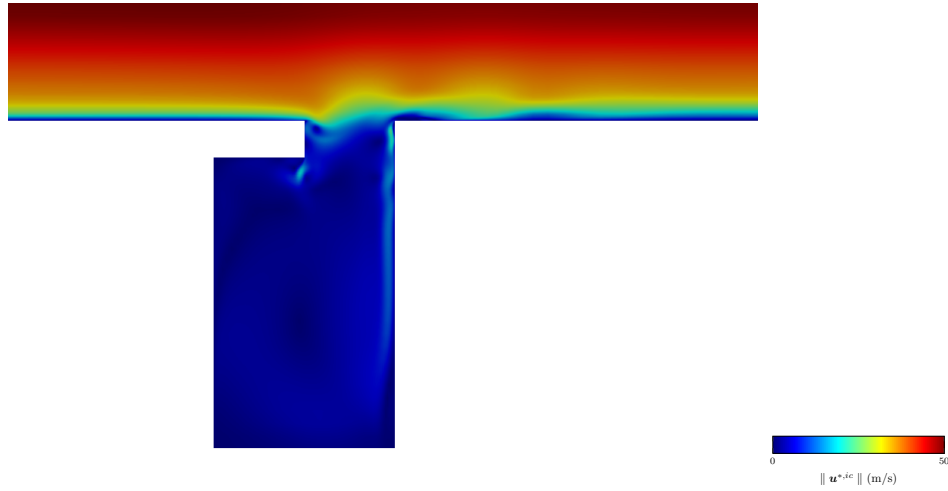


Figure 7. The magnitude of the incompressible component of the velocity captures the vortical flow features of the simulation.

time and frequency domain, and compare it to the measurements inside the cavity as well as outside. In the ideal case, we filter all parts of the radiating field in the aeroacoustic source terms. Therefore, we compare the acoustic field resulting from the corrected source term and the acoustic field forced by the non-corrected source term. Figure 8 illustrates the shape and nature of the Lamb vector and surprisingly there is no visible difference in the source term, except for its strength. The Lamb vector and the derivatives are computed in the framework of radial basis functions.

The acoustic simulation utilizes the equation of vortex sound (11) to compute the acoustic propagation. The Doppler effect is included in the convective property of the wave operator, upstreams the wavefronts reduce their wavelength and downstream the distance between the peaks of the wavefronts are enlarged. The finite element domain consists of three discretization independent and non-conforming regions, connected by non-conforming Nitsche-type Mortar interfaces.²¹ The acoustic sources are prescribed in the source domain and a final outer perfectly matching layer ensures accurate free field radiation. Two different aeroacoustic source variants are investigated, the uncorrected Lamb vector $\mathbf{L}(\mathbf{u})$ (field quantities directly from the flow simulation) and the corrected Lamb vector $\mathbf{L}(\tilde{\mathbf{u}})$ based on the Helmholtz-Hodge decomposition in the vector potential formulation. Figure 9 compares the resulting acoustic field whether applying the source term correction or not. As expected, the acoustic field of the corrected source term is weaker. The corrected acoustic field represents the pure acoustics due to the vortical velocity component in the source term.

Considering the experimental investigation, the sound pressure level inside and outside the cavity is

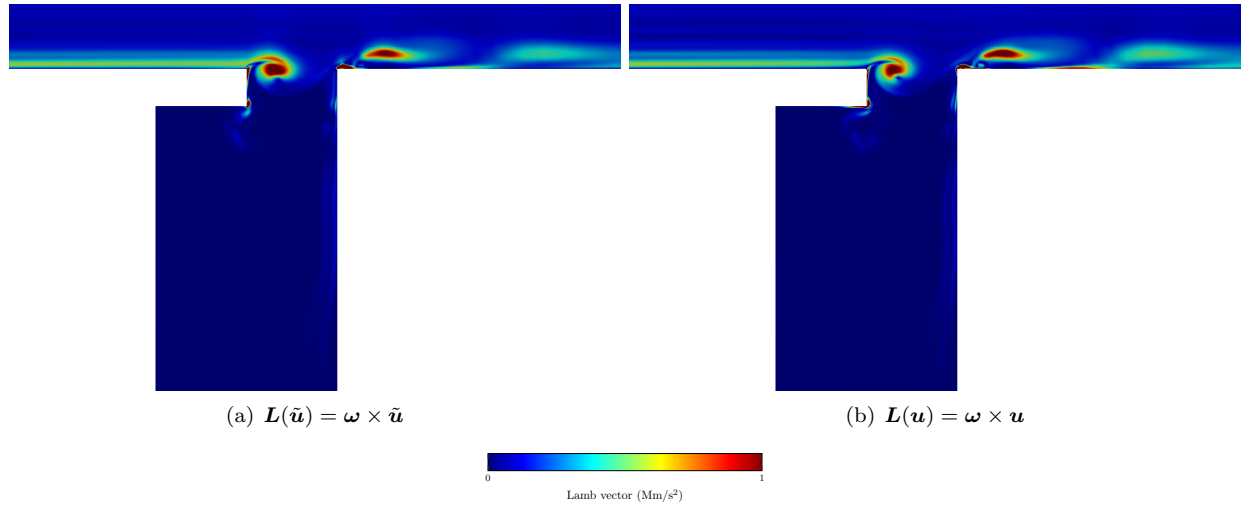


Figure 8. Comparison of the Lamb vector for the corrected and the non-corrected calculation.

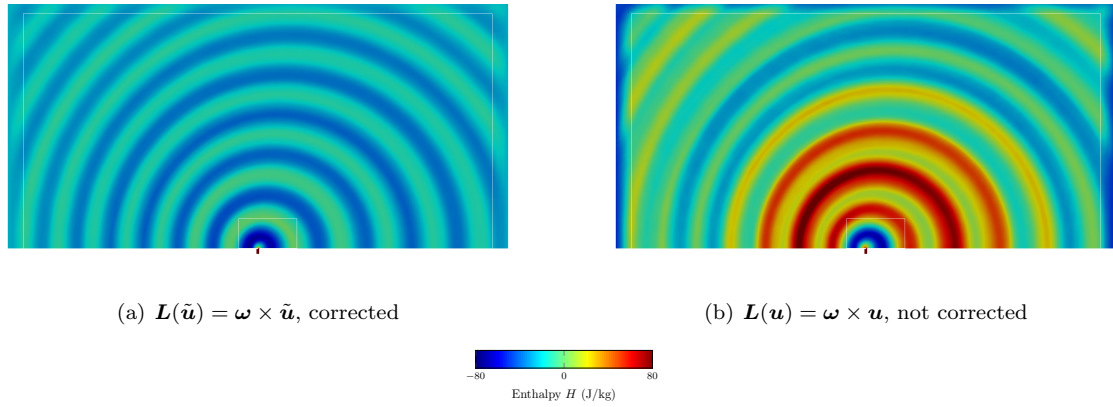


Figure 9. Field of the total enthalpy fluctuation H at a characteristic time. (a) Aeroacoustic sources of the wave equation are due to a compressible flow simulation applying the correction. (b) Aeroacoustic sources are due to a compressible flow simulation without applying the correction equation.

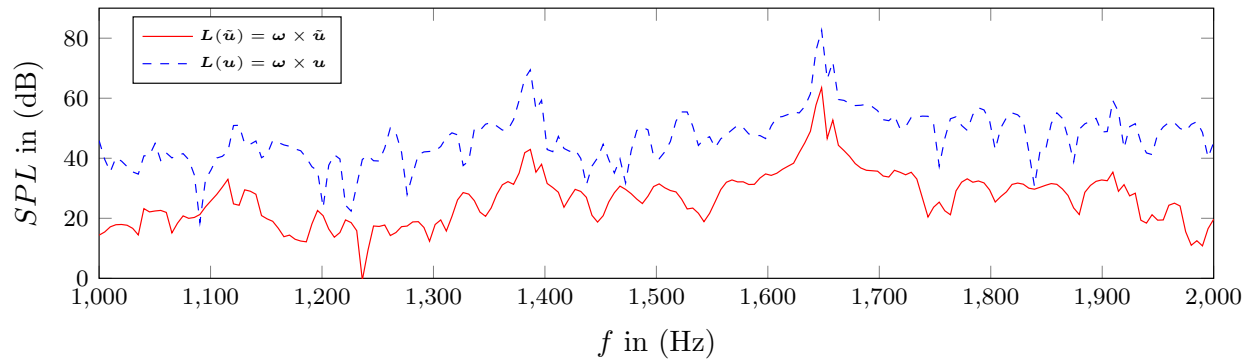


Figure 10. Comparison of the sound pressure level inside the cavity. The curves reveal that both physical peaks are present inside the cavity.

validated. The results meet the expectations for the physical shear layer resonance and the monopole radiation characteristics.^{22–24} Equation (10) and the ideal gas law serves us a relation between the specific

	f_{s1}/Hz	SPL_d/dB	f_d/Hz	SPL_d/dB
Experiment	1650	60.5	1350	52
Simulation $\mathbf{L}(\tilde{\mathbf{u}}) = \boldsymbol{\omega} \times \tilde{\mathbf{u}}$	1660	63	1390	41
Simulation $\mathbf{L}(\mathbf{u}) = \boldsymbol{\omega} \times \mathbf{u}$	1660	83	1390	68

Table 1. Comparison of the pressure inside the cavity

enthalpy and the sound pressure level in its linearized form for $H/R_s T \ll 1$

$$SPL = 20 \log \left(\frac{H}{R_s T p_0} \right). \quad (27)$$

A comparison of the sound pressure level inside the cavity shows that the non-corrected results are higher. The curves in Fig. 10 reveal that both physical peaks are present inside the cavity. The result coincides with the experiment with respect to the location and the amplitude of the resonances, as well as the derived monopole characteristics. A quantitative comparison is given in Tab. 1, where the overall results of the non-corrected acoustic simulation is worse. Speaking of the corrected results we can state that, the characteristic frequencies are captured well, whereas the amplitudes match at the first shear layer mode. The amplitude of the depth mode is underestimated by the simulation results. For the depth mode the discrepancy can be interpreted by the microphone measurements, which recognize the overall pressure fluctuation including the fluid dynamic pressure.

Again the non-corrected results are higher and interestingly, the first mode (1400Hz) is reduced significantly in the corrected formulation as it was found in the experiments. The curve in Fig.11 reveals that only the shear layer mode is significant outside the cavity. The result of the corrected Lamb vector formulation

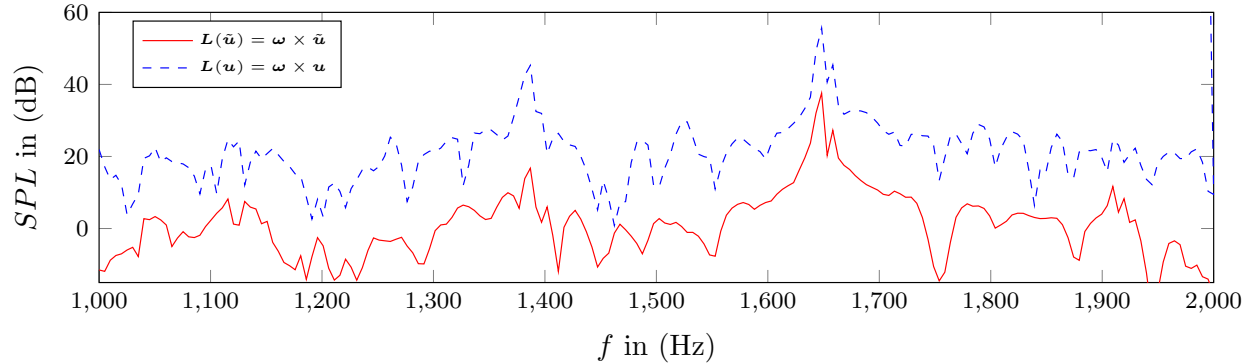


Figure 11. Comparison of the sound pressure level outside the cavity. The curve of the corrected Lamb vector formulation reveals that only the shear layer mode is present outside the cavity.

coincides with the experiment with respect to the location and the amplitude of the resonances. Table 2 quantifies the obtained results in the farfield. Again the characteristic resonances are captured well, and the amplitude of the resonance at depth mode is captured well. The amplitude of the shear layer mode is overestimated, which can be explained by the higher free stream velocity in the simulation.

	f_{s1}/Hz	SPL_d/dB	f_d/Hz	SPL_d/dB
Experiment	1650	30	1350	17
Simulation $\mathbf{L}(\tilde{\mathbf{u}}) = \boldsymbol{\omega} \times \tilde{\mathbf{u}}$	1660	38	1390	19
Simulation $\mathbf{L}(\mathbf{u}) = \boldsymbol{\omega} \times \mathbf{u}$	1660	56	1390	45

Table 2. Comparison of the pressure outside the cavity

V. Conclusions

The crucial difference to state of the art aeroacoustic techniques is that this method handles compressible source data to compute the aeroacoustic source terms. Since a compressible flow simulation already contains acoustics (which are solved by the aeroacoustic analogy), the sources of an aeroacoustic analogy have to be filtered such that a non-radiating base flow is obtained to construct the source terms. We show, that with the help of a Helmholtz-Hodge decomposition, it is possible to extract the vortical (non-radiating) flow component for arbitrary domains. Furthermore, the method filters domain resonant artifacts, due to the boundaries. It has to be noted, that for bounded domains and domains with holes, an additional decomposition component arises, which is in the harmonic function space. The additional harmonic term is the solution of the potential flow theory of the geometrical configuration. As we rely on the divergence free formulation, the equation to obtain the vector potential serves as a valid formulation to extract all divergence-free parts of the flow (whether or not containing harmonic components). The final validation example shows remarkable results for the SPL inside and outside the cavity and the characteristics of the monopole radiation is captured well.

References

- ¹M.J. Lighthill; On sound generated aerodynamically I. General theory. *Proceedings of the Royal Society of London*, (A 211):564-587, 1952.
- ²M. J. Lighthill; On sound generated aerodynamically II. Turbulence as a source of sound. *Proceedings of the Royal Society of London*, (A 222):122, 1954.
- ³H. S. Ribner; Aerodynamic Sound From Fluid Dilatations - A Theory of the Sound from Jets and Other Flows. *UTIA Report No. 86, Institute for Aerospace Studies, University of Toronto*, 1962.
- ⁴C. Bogey, C. Bailly, D. Juvé; Computation of flow noise using source terms in linearized Euler's equations. *AIAA Journal*, Vol. 40 235-243, 2002.
- ⁵Ewert, R. and Schröder, W., "Acoustic Perturbation Equations based on Flow decomposition via Source Filtering," *J. Comp. Phys.*, Vol. 188, 2003, pp. 365-398.
- ⁶W. De Roeck, W. Desmet; Accurate CAA-Simulations using a Low-Mach Aerodynamic/compressible Splitting Technique. In: *15th AIAA/CEAS Aeroacoustic Conference (30th AIAA Aeroacoustic Conference)*. 2009. (p. 3230).
- ⁷M. E. Goldstein; A generalized acoustic analogy. *Journal of Fluid Mechanics*, 488, 315-333, 2003.
- ⁸B. Farkas, G. Pal; Numerical Study on the Flow over a Simplified Vehicle Door Gap - an Old Benchmark Problem Is Revisited. *Period. Polytech. Civil Eng.*, (59)3, 337-346, 2015.
- ⁹S. J. Schoder, M. Kaltenbacher; Aeroacoustic source term filtering based on Helmholtz decomposition. In *23rd AIAA/CEAS Aeroacoustics Conference* 2017. (p. 3696).
- ¹⁰D. G. Crighton; Computational aeroacoustics for low mach number flows. In *Computational Aeroacoustics (ed. J. C. Hardin & M. Y. Hussani)*, Springer, 1993
- ¹¹O. M. Phillips; On the generation of sound by supersonic turbulent shear layers. *J. Fluid Mech.* 9, 1-28, 1960
- ¹²G. M. Lilley; On the noise from jets, AGARD CP-131, 1974
- ¹³M. E. Goldstein; Aeroacoustics. McGraw-Hill, 1976
- ¹⁴Seo, J. and Moon, Y., "Perturbed Compressible Equations for Aeroacoustic Noise Prediction at Low Mach Numbers," *AIAA Journal*, Vol. 43, 2005, pp. 1716-1724.
- ¹⁵Munz, C., Dumbser, M., and Roller, S., "Linearized acoustic perturbation equations for low Mach number flow with variable density and temperature," *Journal of Computational Physics*, Vol. 224, 2007, pp. 352 - 364.
- ¹⁶M. Kaltenbacher, A. Hüppe, A. Reppenhagen, F. Zenger, S. Becker; Computational Aeroacoustics for Rotating Systems with Application to an Axial Fan. *AIAA* 2017
- ¹⁷M. S. Howe. Theory of Vortex Sound. *Cambridge Texts in Applied Mathematics*, 2003.
- ¹⁸B. Henderson; Automobile Noise Involving Feedback- Sound Generation by Low Speed Cavity Flows, In: *Third Computational Aeroacoustic(CAA) Workshop on Benchmark Problems*, Vol. 1, 2000.
- ¹⁹T. Seitz; Experimentelle Untersuchungen der Schallabstrahlung bei der Überströmung einer Kavität. *Diploma Thesis Friedrich Alexander Universität Erlangen*, Supervisor: S. Becker, 2005.
- ²⁰M. Kaltenbacher: Numerical Simulation of Mechatronic Sensors and Actuators: Finite Elements for Multiphysics. Springer, 3rd ed., 2015.
- ²¹M. Kaltenbacher, A. Hüppe, J. Grabinger, B. Wohlmuth; "Modeling and Finite Element Formulation for Acoustic Problems Including Rotating Domains"; *AIAA Journal*, Vol. 54 (2016)
- ²²Y. J. Moon, et al.; Aeroacoustic computations of the unsteady flows over a rectangular cavity with a lip. In: *Third Computational Aeroacoustic(CAA) Workshop on Benchmark Problems*, Vol. 1, 2000.
- ²³Y. J. Moon, et al.; Aeroacoustic tonal noise prediction of open cavity flows involving feedback. *Computational mechanics* (31)3, 359-366. 2003.
- ²⁴G. B. Ashcroft, K. Takeda, X. Zhang; Computations of self-induced oscillatory flow in an automobile door cavity. In: *Third Computational Aeroacoustic(CAA) Workshop on Benchmark Problems*. Vol.1, 2000.